Journal of Power Sources 194 (2009) 1043–1052

Contents lists available at ScienceDirect

Journal of Power Sources

journal homepage: www.elsevier.com/locate/jpowsour

In situ electrochemical synthesis of lithiated silicon–carbon based composites anode materials for lithium ion batteries

Moni Kanchan Datta[a], Prashant N. Kumta[a,b,c,*]

[a] *Bioengineering, Swanson School of Engineering, University of Pittsburgh, PA 15261, United States*
[b] *Bioengineering, Chemical and Petroleum Engineering, Mechanical Engineering and Materials Science, Swanson School of Engineering, University of Pittsburgh, PA 15261, United States*
[c] *Bioengineering, Chemical and Petroleum Engineering, Mechanical Engineering and Materials Science, School of Dental Medicine, University of Pittsburgh, PA 15261, United States*

ARTICLE INFO

Article history:
Received 21 May 2009
Received in revised form 12 June 2009
Accepted 12 June 2009
Available online 21 June 2009

Keywords:
Anode
Lithium ion
Silicon
Carbon
Nanocomposite

ABSTRACT

Most composite anode systems research on lithium ion batteries to date focus on pristine unalloyed Si as the electrochemically active component combined with a suitable matrix component that is electrochemically inactive or relatively inactive to lithium ions. Herein, we report the generation of composites by electrochemical synthesis *in situ*, denoted as Li–Si/C based on Li–Si alloys synthesized as dispersoids in a carbon (C) matrix, as potential anode materials for lithium ion batteries. The electrochemical performance of the Li–Si/C composite of different compositions generated has been systematically studied in order to identify a suitable Li–Si–C composition that could be most effective as a lithium ion anode. The resultant alloy would also exhibit stable electrochemical capacities while expecting to deliver high energy density during discharge with suitable cathode systems. This study shows that the Li–Si/C composite of composition 64 at.% C–21.6 at.% Li–14.4 at.% Si, comprised of Li–Si alloy of compositions in the vicinity of Li–40 at.% Si dispersed in the C matrix cycled within the stable potential window of 0.02–0.5 V, has the potential characteristics of being a promising anode material displaying excellent capacity retention (~0.13% loss per cycle) with high specific capacity (~700 mA h g^{-1}), and also expected to deliver high energy density during discharge in the full cell configuration employing a suitable cathode.

1. Introduction

Rechargeable lithium ion batteries comprised of silicon or silicon alloys as an anode in recent years has gained tremendous interest due to its high theoretical specific capacity (~4212 mA h g^{-1}) corresponding to the formation of a high lithium content intermetallic ($Li_{22}Si_5$) or an amorphous phase of equivalent composition Li–18.5 at.% Si [1–3]. Therefore, Si based anodes render themselves useful for possible application in modern portable electronic devices as well as the much anticipated use in electric/hybrid electric vehicles due to the expected significantly improved gravimetric capacity and energy density in comparison with currently used lithium ion batteries based on utilizing carbon anodes [1–4]. However, the Si based anode materials with the characteristic high specific capacity undergo a large volume expansion and contraction (~2–4 times) during electrochemical cycling due to the repeated alloying and dealloying processes of Si with lithium ions to form intermetallic or amorphous phases containing high lithium content [1–5]. This large volume expansion/contraction as is known leads to catastrophic structural failure of the Si based electrodes during repeated alloying and dealloying cycling processes of Li ions with Si, and as a result the Si based anode materials show poor capacity retention due to eventual loss of electrical contact between the cracked and isolated Si particles, and the current collector [1–7]. This instability ultimately results in failure of the anode and eventually the entire battery. In order to improve the structural stability of the electrode (i.e. capacity retention) of Si based anode materials, the concepts of generating active–inactive or active-relatively active composites *ex situ* as well as electrochemically *in situ* has been explored in great detail primarily to improve the mechanical properties and electronic conductivity of the composite materials wherein the electrochemically active Si is homogeneously dispersed and distributed within a suitable matrix [1,8–20]. The inactive or relatively active matrix is expected to display excellent mechanical strength which can accommodate the mechanical stresses and strains experienced by the active Si phases during the alloying and dealloying processes. In addition, the matrix as well as the electrochemically active phase must possess high

* Corresponding author at: Departments of Bioengineering, Chemical and Petroleum Engineering, Mechanical Engineering and Materials Science, University of Pittsburgh, PA 15261, United States. Tel.: +1 4126480223; fax: +1 4126248069.
E-mail address: pkumta@pitt.edu (P.N. Kumta).

0378-7753/$ – see front matter © 2009 Elsevier B.V. All rights reserved.
doi:10.1016/j.jpowsour.2009.06.033

Table 1
Intermetallic lithium silicides with their molar volume (V_m) and the volume expansion ($(V_m - V_{Si})/V_{Si}$) per mole of Si along with the theoretical specific capacity, and the reported equilibrium discharge and charge potential [1,22–24] associated with the formation of respective phases by alloying of lithium with silicon.

Intermetallics	V_m (cm^3 $mole^{-1}$)	$(V_m - V_{Si})/V_{Si}$ (%)	Gravimetric capacity (mA h g^{-1})	Volumetric capacity (mA h cm^{-3})	Equilibrium discharge potential (V)	Equilibrium charge potential (V)
$Li_{12}Si_7$	26.21	~117	~1641	~1757	0.332	0.58
Li_7Si_3	31.00	~157	~2234	~2023	0.288	0.52
$Li_{13}Si_4$	40.53	~236	~3111	~2155	0.158	0.428
$Li_{22}Si_5$	49.62	~311	~4212	~2383	0.044	0.300

V_{Si} is the molar volume of Si (~12.06 cm^3 mol^{-1}).

electronic conductivity and high lithium ion diffusivity in order to achieve high rate capability. In this regard, different types of Si based composites have recently been generated and investigated [1,8–20]. These systems, synthesized with different kinds of matrices utilizing a variety of synthesis techniques, show improved cyclability with respect to pure silicon [1,8–20] primarily due to the enhancement in the mechanical properties and electronic conductivity. Despite these recent reports [1,8–20], the capacity retention of the Si based anode materials using the composite structures utilizing crystalline, nanocrystalline or amorphous silicon as the dispersoid is still not suitable for use in commercial applications due to the high degree of capacity fade per cycle (>0.1% loss per cycle).

Therefore, in addition to improving the mechanical properties of the Si based materials systems, there is a stringent need to reduce the volume expansion/contraction during repeated alloying and dealloying processes of Si with Li ion in order to obtain long term stability of the Si based anode. These aspects pose a formidable challenge to materials scientists and electrochemists. Table 1 lists the intermetallic lithium silicides in the Li–Si system expected to be formed under equilibrium conditions following the Li–Si binary phase diagram [21]. Table 1 also shows the expected theoretical volume expansion per mole of Si, and the associated theoretical specific capacity characteristic of the different equilibrium Li–Si based intermetallics formed during the alloying reaction of Li with Si [1,2,5,22]. As shown in Table 1, even the formation of $Li_{12}Si_7$, an intermetallic with the lowest Li content of composition Li–36.8 at.% Si, is expected to undergo ~117% volume expansion which is more than sufficient to form cracks in the early stages of cycling of the electrode. In order to minimize the volume expansion/contraction during the alloying and dealloying processes, a concept worth exploring is the ability to synthesize highly expanded form of Si crystals or amorphous Si of molar volume (~100–300% higher than the crystalline form of silicon) closer to the molar volume of Li–Si based intermetallics.

Table 2 shows the expected volume expansion per mole of Si during the alloying of Li with Li–Si based intermetallics along with the associated theoretical specific capacity. Table 2 also shows all the possible equilibrium phase fields including the intermediate reaction phases. Table 2 clearly suggests that the volume expansion/contraction during the alloying and dealloying processes could be reduced if the electrochemical cycling is restricted between the Li–Si based intermetallics rather than pure silicon as a starting material. For example, continued reversible alloying and dealloying of Li with $Li_{12}Si_7$ to form $Li_{22}Si_5$ or $Li_{13}Si_4$ is expected to undergo a volume expansion of only ~89% and ~54%, respectively, albeit still retaining a large theoretical specific capacity of ~2571 mA h g^{-1} (~1455 mA h cm^{-3}) and ~1470 mA h g^{-1} (~1018 mA h cm^{-3}), respectively. Similarly, alloying and dealloying of Li with Li_7Si_3 to form $Li_{22}Si_5$ is expected to exhibit a volume expansion of ~60%, while attaining an impressive theoretical capacity of ~1978 mA h g^{-1} (~1119 mA h cm^{-3}). Tables 1 and 2 also show the equilibrium electrochemical potentials of the two phase region reported at 688 K [22–24] during the discharge and charge processes, respectively, which clearly depicts that the operating voltage window would however be reduced ($0.02\,V = V < 1.2\,V$) if the electrochemical cycling could be performed between the lithiated intermetallics rather than pure Si as an anode. For example, reversible alloying and dealloying reaction of Li with $Li_{12}Si_7$ to form $Li_{22}Si_5$ is expected to occur in the potential window of 0.02–0.52 V (Table 2). It must be mentioned here that the electrochemical cycling between the lithiated intermetallics in the reduced voltage range will essentially provide lower specific capacities in comparison to the pure Si anode cycled in the potential window of 0.02–1.2 V. This would therefore be considered to be disadvantageous particularly in the context of the energy density [energy density (W h g^{-1}) = specific capacity (A h g^{-1}) × potential (V)] that can be delivered in the full cell configuration. However, a larger cell potential can be expected to be achieved in the full cell configuration utilizing a smaller and lower potential range Li–Si based intermetallics as an anode. The combined full cell can actually yield higher energy density even though the specific capacity of the anode is reduced. Hence evaluating the silicon composite anode in the reduced electrochemical potential window region could possibly have many benefits for use in practical lithium ion battery applications.

Based on the above logic, it would be of paramount importance to identify a Si based alloy system that will result in minimum volume expansion/contraction during alloying and dealloying processes combined with improved mechanical properties, while being capable of cycling in a narrow potential window in order to obtain a Si based alloy as an anode that can yield high specific capacity and high energy density with excellent cyclability for lithium ion battery application. A careful examination of Table 2 clearly indicates that the best possible phase field, which exhibits a high

Table 2
The theoretical volume expansion and the theoretical specific capacity of per mole of Si to form different equilibrium Li–Si based intermetallics by alloying/dealloying reaction of Li with Li–Si based intermetallics along with equilibrium discharge/charge potential [1,22–24,36].

Phase fields	Total volume expansion (%)	Gravimetric capacity (mA h g^{-1})	Volumetric capacity (mA h cm^{-3})	Equilibrium discharge potential (V)	Equilibrium charge potential (V)
$Li_{12}Si_7 \leftrightarrow Li_7Si_3$	~18.3	~592	~536	0.288	0.520
$Li_{12}Si_7 \leftrightarrow Li_7Si_3 \leftrightarrow Li_{13}Si_4$	~54.3	~1470	~1018	0.288, 0.158	0.520, 0.428
$Li_{12}Si_7 \leftrightarrow Li_7Si_3 \leftrightarrow Li_{13}Si_4 \leftrightarrow Li_{22}Si_5$	~89.3	~2571	~1455	0.288, 0.158, 0.044	0.520, 0.428, 0.30
$Li_7Si_3 \leftrightarrow Li_{13}Si_4$	~30.7	~877	~794	0.158	0.428
$Li_7Si_3 \leftrightarrow Li_{13}Si_4 \leftrightarrow Li_{22}Si_5$	~60.00	~1978	~1119	0.158, 0.044	0.428, 0.30
$Li_{13}Si_4 \leftrightarrow Li_{22}Si_5$	~22.4	~1100	~620	0.044	0.30
$LiSi \leftrightarrow Li_{12}Si_7 \leftrightarrow Li_7Si_3 \leftrightarrow Li_{13}Si_4$	~114.3	~2154	~3198	0.4,0.288, 0.158	–

theoretical specific capacity and low volume expansion per mole of Si, would be $Li_{12}Si_7 \leftrightarrow Li_{22}Si_5$ or $Li_{13}Si_4$, and $Li_7Si_3 \leftrightarrow Li_{22}Si_5$ with an expected operating potential window of 0.02–0.52 and 0.02–0.43 V, respectively. In this regard, the electrochemical behavior of Li–Si alloy of nominal composition Li–*X* at.% Si ($0.30 \leq X < 1$), which is expected to be a phase mixture of $Li_{12}Si_7$ and Si ($0.37 \leq X < 1$) or $Li_{12}Si_7$ and Li_7Si_3 ($0.30 \leq X \leq 0.37$) according to the equilibrium phase diagram [21], would need to be explored as possible anode materials for lithium ion battery application.

Hence in the present study, composites based on Li–Si alloys of different compositions present as dispersoids in carbon (C) matrix, denoted as Li–Si/C, have been synthesized and studied for their electrochemical response in order to identify a suitable Li–Si–C composition in the Li–Si/C composite system as a possible promising lithium ion anode. Accordingly, in the present study, silicon (Si), graphite (Gr) and polyacrylonitrile derived carbon (PC) composite, denoted as Si/C, have been used to synthesize Li–Si/C based composite of different compositions by the electrochemical reaction of Si/C with Li ion in an electrochemical test cell system. The C in Si/C and Li–Si/C composite has been denoted as a mixture of Gr and PC. In recent years, Si/C based composites have been explored by our research group largely generated using high energy mechanical milling (HEMM) of commercially obtained Si and graphite in the presence of polyacrylonitrile (PAN) followed by thermal treatment up to ~1073–1173 K in inert atmospheres [12]. PAN acts as a diffusion barrier between Si and graphite preventing the formation of the undesired electrochemically inactive SiC during mechanical milling as well as after thermal treatment up to ~1073–1173 K in argon. The Si/C composite thus obtained after thermal treatment of the mechanically milled powder shows a high reversible capacity (~600–700 mA h g^{-1} when tested at a current rate of ~160 mA g^{-1}) with excellent cyclability in the potential window of 0.02–1.2 V [12,14]. In the present study, the Si/C based composite generated by HEMM has been used to synthesize the desired Li–Si/C composite instead of pure microcrystalline Si since the Si/C composite is expected to exhibit better cyclability than pure microcrystalline Si as reported by us earlier [12] due to improved mechanical properties and electronic conductivity. In the present article, the Si/C composite, synthesized after thermal treatment of the mechanically milled powder corresponding to nominal composition 42wt.% Gr–28 wt.% Si–30 wt.% PAN, has been used to synthesize electrochemically *in situ* the Li–Si/C composite anode by controlled electrochemical reaction of Li ion with Si/C. The resultant stable Li–Si–C alloy composition generated *in situ* in the Li–Si/C system has thus been identified which could exhibit high specific capacity with excellent cyclability cycled in the narrow potential window. The *in situ* generated Li–Si/C composites in the Li–Si–C system can also be expected to exhibit high discharge energy density in the full cell configuration. Results of these studies followed by recommendations for the appropriate Li–Si–C composition that would yield the desired optimal specific capacity along with high energy density and excellent stability are discussed in the following sections.

2. Experimental details

2.1. Materials synthesis

Mixtures of elemental powders of synthetic graphite (Aldrich, 1–2 μm), Si (Alfa aesar, −325 mesh) and polyacrylonitrile (PAN) of nominal composition 42 wt.% Gr–28 wt.% Si–30 wt.% PAN were subjected to high energy mechanical milling (HEMM) in a high energy shaker mill (SPEX CertiPrep 8000 M) up to 12 h in a stainless steel (SS) vial using 20 SS balls of 2 mm diameter (~20 g) with a ball to powder weight ratio 10:1 following protocols similar to our earlier publications [12,14,15]. Specifically, ~0.6 g of PAN was dissolved in ~10 ml *N*-methylpyrrolidinone (NMP) to form a homogeneous solution. Graphite (~0.84 g), Si (~0.56 g), and the PAN solution were batched in a vial inside an argon filled glove box (Vacuum Atmosphere HE-493, ~0.10 ppm oxygen and ~0.10 ppm moisture) in order to prevent oxidation of the reactive components during milling. The PAN solution keeps the ingredients and the grinding balls completely submerged in the vial. This was necessary to avoid excessive cold welding commonly known to occur during high energy milling; accompanied agglomeration and consequent temperature build up during milling [25] which is deleterious to the overall electrochemical response. In order to decompose the PAN polymer to form PAN derived carbon (PC) leading to the formation of Si/C composite [12], the mechanically milled powders were annealed isothermally at 1073 K for 6 h in an ultrahigh purity argon (UHP-Ar) atmosphere using a heating rate of 10 K min^{-1} and a flow rate of 100 mL min^{-1}.

Li–Si/C composites of different compositions have then been generated *in situ* by the controlled electrochemical reaction of Li ions with the HEMM derived Si/C composite. Prior to the synthesis of the Li–Si/C composite, a precondition treatment of the Si/C electrode has been carried out to fully activate the electrode and also to confirm that a homogeneous Li–Si/C composite would form by controlled electrochemical reaction of Li ion with the HEMM derived Si/C composite. In order to activate the electrode, the HEMM derived Si/C composite was electrochemically discharged/charged for four cycles in the potential window ~0.02–1.2 V with respect to pure lithium at a current rate of ~160 mA g^{-1} (~315 μA cm^{-2}). In this process, high lithium content Li–Si, Li–C or Li–Si–C based alloys (e.g. $Li_{22}Si_5$ and LiC_6) are expected to be formed during the discharge reaction up to ~0.02 V. The high Li content alloy is then expected to be subsequently dealloyed to form amorphous Si (*a*-Si) and C after charging up to 1.2 V, and as a result a composite based on amorphous Si homogeneously dispersed within and on the C matrix is expected to be formed after charging up to ~1.2 V. In order to synthesize a homogeneous Li–Si/C composite of different compositions, the activated *a*-Si/C electrode that was subjected to four cycles as outlined above was discharged up to ~0.02 V to synthesize high lithium content Li–Si, Li–C or Li–Si–C based intermetallics or amorphous phases which was then subsequently charged (dealloying of Li from Li–Si, Li–C or Li–Si–C based intermetallics or amorphous phases) to different potentials (~0.6, ~0.5 and ~0.4 V). The charge cycle was terminated at these three respective potentials, and the corresponding compositions and the phases of the Li–Si/C composite synthesized at ~0.6, ~0.5 and ~0.4 V, respectively, has been determined from the associated specific capacity arising due to the alloying/dealloying reactions of Li with Si/C composite which will be discussed in detail in Section 3.

2.2. Materials and electrochemical characterization

In order to perform qualitative phase analysis, the milled powders as well as the heat treated powders were characterized by X-ray diffraction (XRD) using the Philips XPERT PRO system employing the Cu K_α ($\lambda = 0.15406$ nm) radiation. Electrochemical characteristics of the Si/C composite were analyzed from electrodes that were prepared by mixing 82 wt.% of the active powder of −325 mesh (<44 μm particle size) and 8 wt.% conductive nano-sized (~40 nm) Super P carbon black (TIMCAL). A solution containing 10 wt.% polyvinylidene fluoride (PVDF) in *N*-methylpyrrolidinone (NMP) was added to the mixture. The as-prepared solution was then coated onto a Cu foil and dried in a vacuum oven at 110 °C for 12 h. A 2016 coin cell design was used employing lithium foil as a counter electrode and 1 M $LiPF_6$ in ethylene carbonate/diethyl carbonate (EC/DEC = 1:2 in volume) as the electrolyte. All the cells, based on the HEMM derived Si/C composite, tested in this study were cycled at room temperature (~298 K) within 0.02–1.2 V employing the

discharge/charge rates of ~160 mA g^{-1} with a minute rest period between the charge/discharge cycles using a potentiostat (Arbin electrochemical instrument). On the other hand, the *in situ* generated Li–Si/C composites of different compositions were synthesized at ~0.6, ~0.5 and ~0.4 V, and cycled in their stable potential window of ~0.02–0.60, ~0.02–0.50 and 0.02–0.40 V, respectively, at a current rate of ~160 mA g^{-1}. The compositions of the Li–Si alloy at different potentials has been calculated from the associated specific capacity at that potential determined due to the alloying of Li ion with Si. However, graphite is also expected to contribute to the overall specific capacity of the Si/C composite at a given potential. In order to deconvolute the specific capacity contribution from graphite, multi-peak fitting using the Gaussian function of the overlapping peaks, associated with different phase formation states during the alloying/dealloying processes of Li ion with graphite and Si, observed in the differential capacity plot (d*Q*/d*V*) has been carried out using the OriginPro 7, data analysis and graphing software package (OriginLab Corporation) [26]. The average capacity loss per cycle (%) up to 30th cycle of the electrode has been calculated using the following equation: *capacity loss per cycle* (%) = [(*charge capacity after 30th cycle* − *charge capacity after 1st cycle*) × *100*]/[*total number of cycle* (*30*)].

3. Results and discussion

The XRD patterns of the as-prepared composite precursor of nominal composition 42 wt.% Gr–28 wt.% Si–30 wt.% PAN obtained after 12 h of mechanical milling are shown in Fig. 1. The XRD pattern of the 12 h milled composite precursor shows the presence of only graphite and silicon without any detectable amount of SiC. As expected from our earlier results [12], the formation of electrochemically inactive SiC, which could be easily formed during high energy mechanical milling (HEMM) of pure graphite and silicon [12], is bypassed during mechanical milling using PAN as the polymer additive indicating the effectiveness of PAN to act as a diffusion barrier preventing the reactive diffusion of Si with C forming SiC. The formation of SiC is undesirable since it reduces the amount of electrochemically active Si in the final electrode composition thus reducing the final expected capacity of the electrode. It is also interesting to note that graphite, which would normally transform to the disordered amorphous form during high energy mechanical milling [12], retains its graphitic structure in the presence of PAN even after 12 h of mechanical milling. PAN is thus effective in also diminishing the direct impact of the comminutive action of the milling media with the reactants during high energy milling known to cause the breakdown of the graphitic layered structure. The present results clearly suggest the dual action of PAN, namely, the PAN solution, which is expected to be absorbed and coated on the newly formed surfaces of the particles generated by the processes of repeated cold welding and fracture widely prevalent during mechanical milling, acts as a diffusion barrier to the interfacial diffusion reaction between graphite and Si known to form electrochemically inactive SiC, while also reducing the amorphization kinetics of graphite. Although PAN is useful in preventing the formation of undesirable SiC, its presence in the final product is also undesirable due to the poor electrical conductivity and poor lithium ion diffusivity of PAN which is expected to deteriorate the electrode performance of the Si/C and the *in situ* synthesized Li–Si/C composite. Hence, it is necessary to pyrolyze and convert PAN to an electrically conductive and lithium ion diffusive carbon by thermal decomposition at a suitable temperature. Based on our earlier published differential thermal and thermogravimetric (DTA/TGA) results on PAN [12], the 12 h milled powder has been accordingly thermally treated at ~1073 K for 6 h in UHP Ar atmosphere to decompose PAN to form PAN derived carbon, denoted as PC. The XRD pattern of the powder thermally treated at ~1073 K, also shown in Fig. 1, shows the characteristic peaks corresponding to only graphite and Si as the crystalline phases without any detectable amount of SiC. The final composition of the Si/C composite obtained after thermal treatment at ~1073 K is estimated knowing the ~37% yield of PAN derived carbon [12] determined from thermal analysis and considering no weight loss undergone by graphite and silicon during the inert atmosphere thermal treatment. Based on the thermal analysis results, the composition of the composite is determined to be approximately 51.8 wt.% Gr–34.5 wt.% Si–13.7 wt.% PC, which corresponds to an atomic percent composition of 64.5 at.% Gr–18.4 at.% Si–17.1 at.% PC, where Gr and PC denotes graphite and PAN derived carbon, respectively.

Fig. 2 shows the variation of specific capacity *vs.* cycle number of the Si/C composite cycled at a rate of ~160 mA g^{-1} (~C/6) in the potential window ~0.02–1.2 V. As shown in Fig. 2, the Si/C composite shows an impressive 1st discharge and 1st charge capacity of ~1215 and ~1019 mA h g^{-1}, respectively, with an irreversible loss of only ~16%. The Si/C composite, however, exhibits a ~0.34% loss in capacity per cycle up to 30 cycles, whereas pure microcrystalline Si (*c*-Si) as is well known exhibits rapid fade in capacity within only few cycles (Fig. 2) [1,6]. This result clearly suggests that the use of a polymer and graphite during mechanical milling with Si to form the Si/C composite significantly improves the cyclability and the

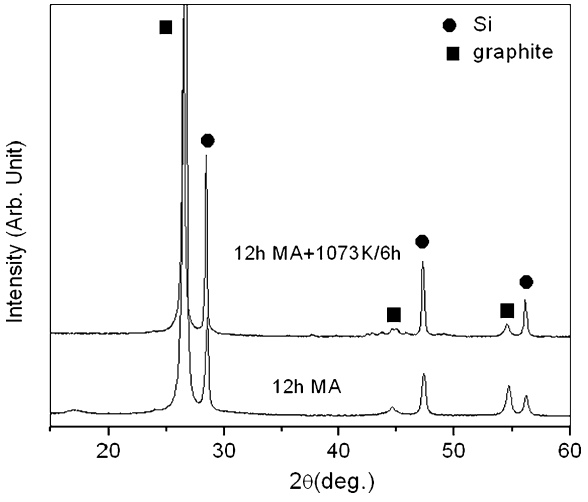

Fig. 1. XRD patterns of 42% C–28 wt.% Si–30 wt.% PAN generated after 12 h of mechanical milling and after thermal treatment of mechanically milled powder at ~1073 K for 6 h in UHP argon.

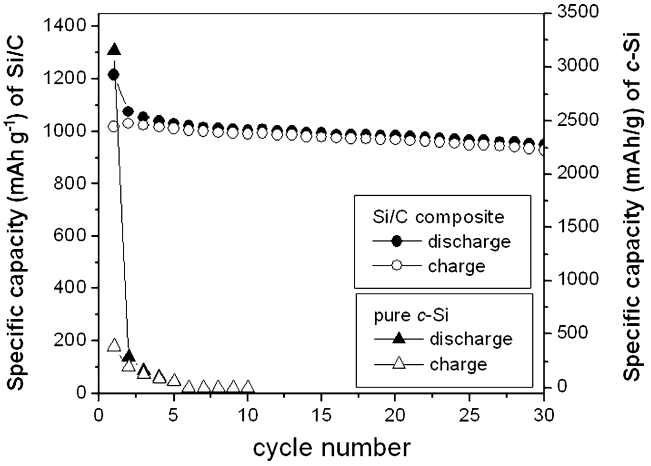

Fig. 2. Specific capacity *vs.* cycle number of Si/C composite and pure microcrystalline Si (*c*-Si) cycled at a constant current of ~160 mA g^{-1} in the potential window of 0.02–1.2 V.

structural stability of Si with respect to pure microcrystalline Si. This improvement in the structural stability of the Si/C composite can be expected as we reported earlier due to the likely improvement in mechanical properties of the composite arising due to the homogeneous dispersion and distribution of Si within the graphite matrix brought about by extended milling [12,14,15]. In addition, the solution coating of graphite and silicon by PAN during milling is expected to enhance the wettability between graphite and Si. As a result, the coating of the graphite and silicon by PAN based amorphous carbon obtained by thermal decomposition of PAN will likely improve the mechanical properties of the composite particularly, by enhancing the interface adhesion and/or bonding between the Si and graphite. The presence of a possible compressive stress on Si exerted by the PAN derived amorphous carbon (PC) has also been recently suggested to be the cause of the perceived stability of the Si/C composite obtained from pyrolysis of polymers [12,18] arising due to the expected likely improvement in fatigue strength of the composite. Thus, the Si/C based composite with the PAN based carbon coating results in improved capacity retention with respect to *c*-Si due to the possible enhancement of the mechanical properties of the resultant composite.

However, despite the improved interface adhesion brought by the use of PAN and the formation of the PAN derived disordered amorphous carbon resulting in average retention in capacity (~0.34% loss per cycle) of Si/C based composite obtained after thermal treatment of mechanically milled powder of nominal composition 42 wt.% Gr–28 wt.% Si–30 wt.% PAN, the system is not likely to be suitable for practical commercial applications requiring further improvements in the cycling stability. In order to further improve the stability of the electrode, various lithiated forms of the Si/C composite, denoted as Li–Si/C, comprised of Li–Si based alloys dispersed on C matrix, has been synthesized *in situ* by controlled electrochemical reaction of Li with the Si/C composite. A reduction in volume expansion or contraction during electrochemical cycling of Li–Si/C composite and as a result, a better cyclability in comparison to pure Si/C composite is expected due to the presence and direct formation of Li–Si based intermetallics or amorphous phase/es in the *in situ* synthesized Li–Si/C composite as discussed in Section 1. In order to identify the favorable Li–Si–C composition that would yield the desired specific capacity combined with high energy density, and also to study the correlation of the cyclability as well as the reversible capacity with specific compositions in the electrochemically synthesized Li–Si/C composite, the phase/phases present and their corresponding composition at different potentials needs to be identified. In this regard, the phase formation/transformation at different potentials and the alloying/dealloying behavior of Li ions with Si/C during discharge/charge processes need to be understood. The phase formation/transformation reactions and the alloying/dealloying behavior of Li ion with the Si/C composite during the discharge/charge processes can be understood in detail by analyzing the differential capacity plot (d*Q*/d*V vs. V*) corresponding to the 1st cycle and 2nd cycle onwards for the synthesized Si/C composite cycled at ~160 mA g^{-1} in the potential window of 0.02–1.2 V.

The differential capacity plot (d*Q*/d*V vs. V*) relating to the 1st cycle of the Si/C composite is shown in Fig. 3. Several researchers [1,2,12,14–19,27–30] have also reported a similar 1st discharge and 1st charge profile for microcrystalline Si based anodes cycled at a moderate current rates (<1C rate). It is clearly evident from Fig. 3 that the alloying reaction (discharge) of Li ion with crystalline Si (*c*-Si) in the Si/C composite occurs mainly at a peak potential of ~0.060 V with an onset potential of ~0.10 V during the 1st discharge. A careful comparison of the reaction potential of the 1st discharge (peak potential ~0.06 V) with the expected equilibrium potential (Table 1) to form the different equilibrium Li–Si based intermetallics during the electrochemical reaction of Li ion with Si,

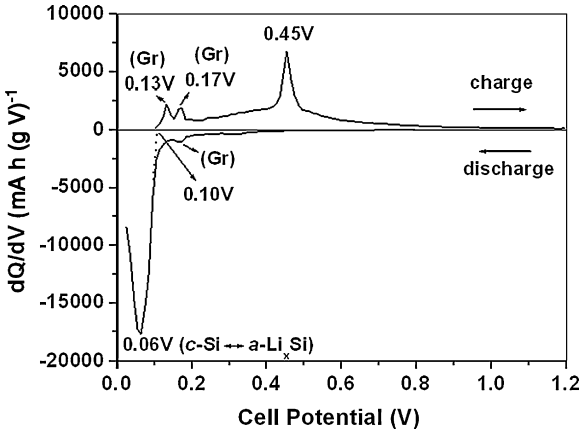

Fig. 3. Differential capacity *vs.* cell potential curves of HEMM derived Si/C composite electrode obtained after 1st cycle cycled at ~160 mA g^{-1} in the potential window of 0.02–1.2 V.

it is clearly evident that the reaction products obtained following the 1st discharge of Li ions with crystalline Si (*c*-Si) at room temperature appears to deviate significantly from equilibrium. Several researchers [2,27–33] have reported that the phase forming at a peak potential close to ~0.06 V with an onset potential ~0.10 V, associated with a long flat plateau during the 1st discharge, corresponds to the formation of metastable Li–Si based amorphous phase (*a*-Li$_x$Si) by a solid state amorphization reaction where the crystallization of the equilibrium intermetallic phases is kinetically forbidden. On the other hand, the differential capacity plot (d*Q*/d*V vs. V*) of the 1st charge (Fig. 3) shows that the dealloying (charging) reaction of Li ion from *a*-Li$_x$Si occurs corresponding to a combination of a broad peak followed by a sharp peak occurring at a peak potential of ~0.45 V. Li and Dahn [27] have reported the formation of amorphous phase (*a*-Li$_z$Si, $z < 2$) by the dealloying reaction of Li ion from *a*-Li$_x$Si corresponding to the onset potential of ~0.41 V with a peak potential ~0.45 V. The formation of amorphous Si (*a*-Si) after complete delithiation (at ~1.2 V) from the lithiated *a*-Li$_x$Si alloy following the initial discharge has been confirmed by several researchers in earlier publications [2,14,27–33]. It can therefore be expected that after complete delithiation of the *a*-Li$_x$Si at room temperature, the Si atoms remain possibly frozen in their atomic positions due to the expected atomic immobility of the Si atoms at room temperature. As a result, the crystalline Si undergoes solid state amorphization due to the large atomic displacement of Si atoms during the alloying reaction causing significant lattice strain and softening of the shear elastic constant leading to the process of mechanical melting [25,34]. More detailed studies are nevertheless needed to determine the exact amorphous structure, atomic coordination, root mean square static atomic displacement and the corresponding molar volume of the amorphous Si (*a*-Si) generated after the delithiation of *a*-Li$_x$Si. In addition, the d*Q*/d*V* curve for the 1st charge also shows two additional dealloying processes occurring at the peak potentials of ~0.13 and ~0.17 V which is known to occur due to the dealloying reaction of Li from Li$_6$C to C [35,36]. Therefore, a composite based on the formation of amorphous Si (*a*-Si) homogeneously dispersed within and on the C matrix, denoted as *a*-Si/C, is expected to be formed after charging up to ~1.2 V in these novel Si/C based nanocomposite systems.

The differential capacity plot (d*Q*/d*V vs. V*) of the 1st cycle of Si/C composite (Fig. 3) shows that both Si and Gr are active. In addition to Si and Gr, the disordered amorphous carbon generated from PAN is also expected to contribute to the overall capacity of the composite. The 1st charge capacities of graphite and PC determined from individual testing of the cells were ~310 and ~320 mA h g^{-1}, respectively, cycled at ~160 mA g^{-1}. On the other

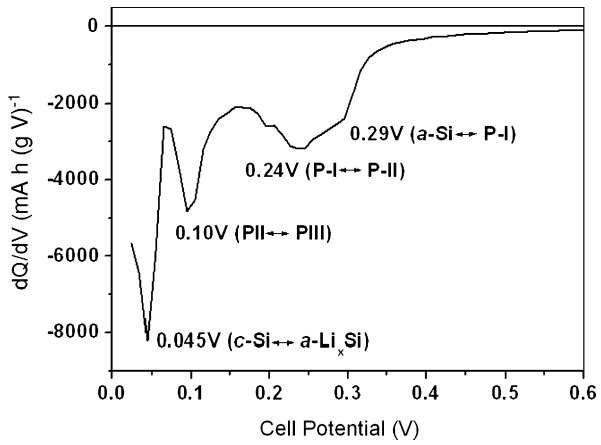

Fig. 4. Differential capacity *vs.* cell potential curves of Si/C composite electrode obtained after the 2nd discharge cycled at ~160 mA g^{-1} in the potential window of 0.02–1.2 V.

hand, the 1st discharge and 1st charge capacities of pure microcrystalline Si (Fig. 2) determined from the individual testing of cells are ~3150 and ~385 mA h g^{-1}, respectively, when cycled at 160 mA g^{-1} (~C/20 rate) which is in good agreement with the earlier reports for microcrystalline Si [1,6,27–29]. The large irreversible loss of pure microcrystalline Si and as a result, the low 1st charge capacity mainly arises from the structural failure of the microcrystalline Si rather than the formation of an SEI layer as is the normal case for most anode systems [1,2,6,27–32]. Chan et al. [2] have recently reported a ~27% irreversible loss of more structurally stable Si nanowires cycled at a similar C/20 rate, and several researchers [7,31,37,38] have reported an irreversible loss ~15–30% for the structurally stable thin film amorphous Si anode (~250 nm thick film) depending on the discharge/charge rate. Therefore, the 1st charge capacity (~384 mA h g^{-1}) of microcrystalline Si observed in the present study could not be considered as the intrinsic 1st charge capacity in calculating the expected contribution of Si in structurally stable Si/C composite. Hence in the present study, the irreversible loss of pure microcrystalline structurally stable Si has been considered to be similar to that of the structurally stable Si nanowires exhibiting an irreversible loss ~27% [2] assuming no significant difference in irreversible loss with moderate change in the charge/discharge rates. In the present study utilizing the results reported for Si nanowires, the expected 1st charge capacity of microcrystalline Si within the structurally stable Si/C composite will therefore be ~2300 mA h g^{-1} with a 1st discharge capacity ~3150 mA h g^{-1}. The expected contribution to the 1st charge capacity of the Si/C composite due to the presence of graphite (51.8 wt.%), PC (13.7 wt.%) and Si (34.5 wt.%) will therefore be approximately ~160, ~44 and ~793 mA h g^{-1}, respectively. Hence, the overall expected capacity of the Si/C composite based on the observed capacities of the individual cells discussed above and that expected and deduced for Si will be ~997 mA h g^{-1} which is in good agreement with the experimentally observed 1st charge capacity (~1019 mA h g^{-1}) of Si/C composite cycled at ~160 mA g^{-1}.

The differential capacity plots (d*Q*/d*V vs. V*) of the 2nd discharge and 2nd charge of the Si/C composite cycled at a rate of 160 mA g^{-1} in the voltage range of 0.02–1.2 V are shown in Figs. 4 and 5, respectively. Similar discharge/charge profiles from the 2nd cycle onwards has been reported for pure *c*-Si and Si/C based composite anodes researched by several researchers [1,2,12–20,27,30] irrespective of the discharge/charge rates. It can be construed from Fig. 4 that from the 2nd cycle onwards, during alloying of lithium ions with *a*-Si/C, generated after delithiation of *a*-Li$_x$Si and LiC$_6$, nucleation and growth of other intermetallics/amorphous phase/es corresponding to the peak potentials, ~0.29, ~0.24 and ~0.10 V appear to occur, respectively. Similar peak profiles and peak potentials have been reported from the 2nd discharge cycle onwards for thin films of amorphous Si [7,37,38] as well as for bulk amorphous Si [31] which validate the observed reaction potentials in the present study corresponding to the reaction of *a*-Si with Li ions. In addition, Fig. 4 also shows the formation of *a*-Li$_x$Si at the peak potential ~0.045 V similar to 1st discharge reaction shown in Fig. 3 due to the lithiation of *c*-Si. In the present study, the phase/es forming corresponding to the peak potential ~0.29, ~0.24 and ~0.10 V has been denoted as phase P-I, P-II and P-III, respectively. The composition of the P-I, P-II and P-III, phases estimated based on the associated specific capacity of the respective phase related to the number of reacting lithium ions, is corresponding to Li–50 at.% Si (LiSi), Li–30 at.% Si(Li$_7$Si$_3$) and Li–24 at.% Si (Li$_{3.16}$Si), respectively. On the other hand, the differential capacity plot (d*Q*/d*V vs. V*) obtained for the 2nd charge (Fig. 5) shows the processes of dealloying from the phase corresponding to P-III to form *a*-Si as well as dealloying of *a*-Li$_x$Si and LiC$_6$ to *a*-Si and C, respectively, similar to the 1st charge reaction shown in the differential capacity plot in Fig. 3. In order to identify the peak profile, and the onset and offset potential corresponding to the formation of the different phase/es as well as the associated specific capacity (determined from the area under the curves) related to a certain precise phase formation, multi-peak fitting has been conducted employing the Gaussian function of the overlapping peaks associated with the 2nd charge using the OriginPro 7 software package [25,26] as outlined in Section 2. The deconvoluted peaks observed at the peak potential ~0.28 and ~0.47 V are similar in nature to that reported for amorphous Si thin films as well as for bulk amorphous Si arising from the 2nd cycle onwards [7,31,37,38]. A careful comparison of the onset potential of the 2nd discharge and 2nd charge, shown in Figs. 4 and 5, and also calculated from associated specific capacity corresponding to the different phase transformation reactions, it can be concluded that the dealloying of Li ion from P-III to P-II occurs corresponding to the onset potential ~0.16 V which is the potential where phase P-III exists in its pure form as shown in Fig. 5 and remains in the two phase region (P-III and P-II) in the wide potential range of ~0.16–0.4 V with a peak potential ~0.28 V, and transforms completely to P-II phase at ~0.4 V.

On the other hand, dealloying of Li ion from P-II to P-I occurs corresponding to the onset potential ~0.40 V as shown in Fig. 5, and coexists in the potential range of 0.40–0.62 V with a peak potential ~0.47 V, and transform fully to P-I phase at ~0.62 V. However, it must be mentioned here that no significant peak in the differential capacity (d*Q*/d*V*) curve of 2nd charge (Fig. 5) corresponding to the transformation of the P-I phase to form *a*-Si is noticeable, and this

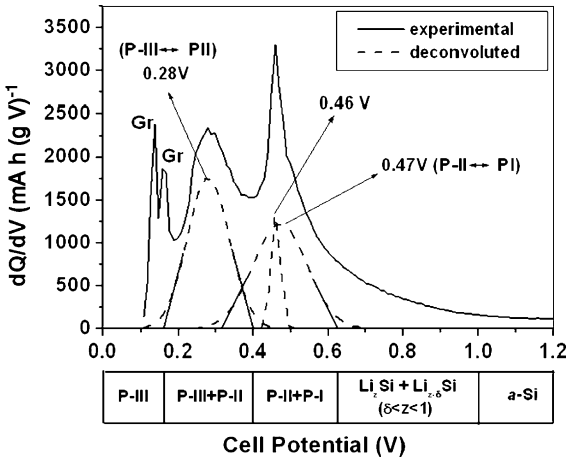

Fig. 5. Differential capacity *vs.* cell potential curves of HEMM derived Si/C composite electrode obtained after the 2nd charge cycled at ~160 mA g^{-1} and the expected metastable phase diagram at room temperature with cell potential shown below.

may be due to the high discharge/charge rates of 160 mA g^{-1} (~C/6) employed in the present study. Based on the above consideration, the phase transformation reactions observed during alloying and dealloying of the Si/C composite formed by high energy mechanical milling (HEMM) in the present study most likely involve formation of metastable phases. The probable metastable phase fields present at room temperature as a function of the potential during delithiation of P-III to form *a*-Si from the 2nd cycle onwards are shown below in the differential capacity plot in Fig. 5 as a bar diagram. The detailed phase formation and phase transformation mechanisms occurring during lithiation and delithiation of crystalline Si as well as amorphous Si will be published in another publication very shortly.

The metastable Li–Si phase diagram, shown as a bar diagram below in Fig. 5, shows the expected phase/phases and phase fields at different potentials. For example, pure phase P-I and P-II of composition Li–50 at.% Si (LiSi) and Li–30 at.% Si (Li_7Si_3), respectively, is expected to form at ~0.6 V and ~0.4 V, respectively, during dealloying of Li from P-III and *a*-Li_xSi. However, a mixture of P-I and P-II phase is expected to form at a potential of ~0.5 V during dealloying of P-III and *a*-Li_xSi. On the other hand, pure C is expected to form after dealloying of LiC_6 in the above potential ranges as shown in Figs. 3 and 5. From the above considerations, it is very clear that a Li–Si alloy dispersed on C matrix, denoted as Li–Si/C composite, could be generated *in situ* by terminating the charging reaction of the Si/C composite electrode at different potentials. In this respect, a precondition treatment of Si/C electrode, by cycling the electrode between 0.02 and 1.2 V for the first four cycles, has been carried out to fully activate the electrode and to confirm that a homogeneous Li–Si/C composite would form following termination of the subsequent dealloying reactions at different potentials. In order to electrochemically synthesize *in situ* the Li–Si/C composite of different compositions, the electrochemical charging of the activated Si/C composite electrode has been terminated at ~0.6, ~0.5 and ~0.4 V. The Li–Si/C composite thus generated *in situ* at ~0.6 V is expected to be comprised of pure P-I phase of composition Li–50 at.% Si (LiSi) (Fig. 5) dispersed homogeneously in the C matrix which is corresponding to the overall composition of 69 at.% C–15.5 at.% Li–15.5 at.% Si. Fig. 6 shows the electrochemical performance of the Li–Si/C composite, electrochemically synthesized *in situ* at ~0.6 V, cycled in the stable potential window ~0.02–0.6 V at a rate of ~160 mA h g^{-1}. It must be mentioned here that the 1st cycle discharge capacity, shown in Fig. 6, corresponds to the discharge capacity of the activated Si/C composite initially cycled in the potential window of 0.02–1.2 V for four cycles. The Li–Si/C composite, thus electrochemically generated *in situ* at ~0.6 V and cycled in the voltage range of ~0.02–0.6 V at a rate of 160 mA g^{-1}, shows a 1st charge capacity of ~819 mA h g^{-1} which is expectedly ~19.6% lower than the 1st charge capacity (~1019 mA h g^{-1}, Fig. 2) obtained for the pure Si/C composite cycled in the ~0.02–1.2 V voltage window range. The capacity retention of the Li–Si/C composite, synthesized *in situ* at ~0.6 V, however has been improved to ~0.21% loss per cycle in comparison to ~0.34% loss per cycle of Si/C composite cycled in the ~0.02–1.2 V potential window.

In contrast to the Li–Si/C composite synthesized electrochemically when the charge cycle is terminated at ~0.6 V, the Li–Si/C composite obtained at ~0.5 V is expected to be comprised of P-I and P-II phase mixture (Fig. 5) of composition Li–50 at.% Si (LiSi) and Li–30 at.% Si (Li_7Si_3), respectively, dispersed homogeneously in the C matrix. The overall composition of the Li–Si alloy generated at ~0.5 V calculated from the associated specific capacity at ~0.5 V is close to Li–40 at.% Si which is corresponding to the overall composition 64 at.% C–21.6 at.% Li–14.4 at.% Si in the electrochemically *in situ* generated Li–Si/C composite. The Li–Si/C composite, obtained at ~0.5 V, cycled at a rate of ~160 mA g^{-1} in the potential window of 0.02–0.5 V (Fig. 6) shows a 1st charge capacity of ~700 mA h g^{-1}. The 1st charge capacity of Li–Si/C obtained at ~0.5 V, cycled in the potential window of 0.02–0.5 V, is around 31.3% lower than the 1st charge capacity of the pure Si/C composite cycled between ~0.02 and 1.2 V shown in Fig. 2. However, the capacity retention of the Li–Si/C composite obtained at ~0.5 V is significantly improved (~0.13% loss per cycle) with respect to Li–Si/C composite generated at ~0.6 V (~0.21% loss per cycle) and pure Si/C composite (~0.34% loss per cycle) cycled within their stable potential window at the identical rate of ~160 mA g^{-1}. The columbic efficiency of the Li–Si/C obtained at ~0.5 V, plotted in Fig. 6, increases from ~97% at 2nd cycle to ~99% after 5th cycle, and remains above ~99% in the subsequent cycles up to 30 cycles. The electrochemically *in situ* generated Li–Si/C composite, obtained at ~0.4 V, cycled at a rate of ~160 mA g^{-1} in the potential window ~0.02–0.4 V, shows a 1st charge capacity of ~443 mA h g^{-1} although exhibiting a fade in capacity ~3.6% loss per cycle (Fig. 6) within 10 cycles. Furthermore, the capacity retention of Li–Si/C composite obtained at ~0.4 V is however significantly deteriorated (~3.6% loss per cycle) with respect to the Li–Si/C composite obtained electrochemically *in situ* at ~0.6 V (~0.21% loss per cycle) and ~0.5 V (~0.13% loss per cycle), respectively. The 1st charge capacity of the Li–Si/C obtained electrochemically *in situ* at ~0.4 V, cycled in the potential window of

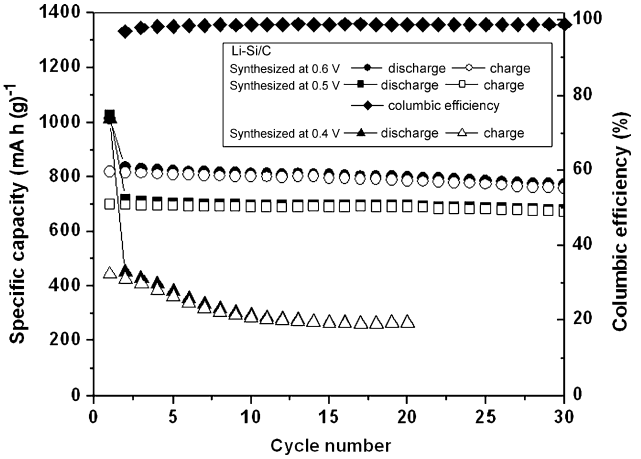

Fig. 6. Specific capacity *vs.* cycle number of Li–Si/C composite, synthesized after termination of the electrochemical charging reaction of Li ion with activated Si/C composite at ~0.6 V, ~0.5 V and ~0.4 V, respectively, cycled within their stable potential window at a constant current of ~160 mA g^{-1}. The columbic efficiency for the cell cycled in the 0.02–0.5 V window is also shown.

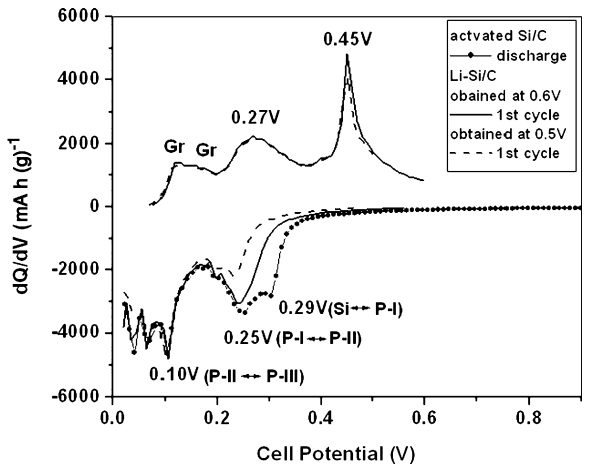

Fig. 7. Differential capacity *vs.* cell potential plot of Li–Si/C composite electrode electrochemically synthesized *in situ* after termination the electrochemical charging reaction of Li ion with activated Si/C composite at ~0.6 and ~0.5 V, and cycled at ~160 mA g^{-1} within their stable potential window.

0.02–0.4 V, is approximately 56.5% lower than the 1st charge capacity corresponding to the pure Si/C composite cycled in the potential window of 0.02–1.2 V. According to the estimated metastable Li–Si phase diagram (Fig. 5), the *in situ* generated Li–Si/C composite obtained at ~0.4 V is expected to be comprised of pure P-II phase of composition close to Li–30 at.% Si (Li_7Si_3) with an overall composition 57.1 at.% C–30 at.% Li–12.9 at.% Si in the *in situ* generated Li–Si/C composite.

The differential capacity plots corresponding to the 1st cycle of the electrochemically *in situ* generated Li–Si/C composite following termination of the electrochemical cycle at ~0.6 and ~0.5 V along with the discharge cycle of activated Si/C composite electrode after the first four cycle activation to ensure formation of amorphous Si (*a*-Si) described above are shown in Fig. 7. The d*Q*/d*V* plots (Fig. 7) of the *in situ* generated Li–Si/C composite electrode synthesized after terminating the charge cycle at ~0.6 and ~0.5 V followed by cycling in the potential window ~0.02–0.6 and ~0.02–0.5 V, respectively, show that the peak corresponding to the formation of the P-I phase with a peak potential ~0.29 V is bypassed which clearly suggests that no further P-I phase is formed during lithiation of the *in situ* generated Li–Si/C composite synthesized electrochemically at ~0.6 and ~0.5 V, respectively. This result also confirms that there is no free *a*-Si present in the *in situ* generated Li–Si/C composite, synthesized at ~0.6 and ~0.5 V, to form any additional P-I phase by electrochemical reaction of Li ion with the electrochemically generated *in situ* Li–Si/C composite, which is in good agreement with the expected phase/es at ~0.6 V (P-I) and ~0.5 V (P-I + P-II) shown in the metastable phase diagram in Fig. 5. In addition, it has been noticed that the peak intensity of d*Q*/d*V* curve corresponding to the formation of the P-II phase (~0.25 V) decreases with a decrease in the termination potential from ~0.6 to ~0.5 V to generate the Li–Si/C composite. This result can be understood by considering that the weight fraction of P-II phase increases whereas the weight fraction of P-I phase decreases with a decrease in the termination potential (from 0.6 to 0.5 V) of the synthesized Li–Si/C composite which is also in agreement with the metastable Li–Si phase diagram shown in Fig. 5. On the other hand, the differential capacity plot (d*Q*/d*V vs. V*) for the 1st, 5th and 8th cycles of *in situ* synthesized Li–Si/C composite generated electrochemically at ~0.4 V cycled at the same current of ~160 mA g^{-1} in the potential window of 0.02–0.4 V, shown in Fig. 8, indicates that the peak corresponding to the formation of P-II phase (peak potential ~0.25 V during discharge, Fig. 4) no longer exists. This result clearly suggests that there is no P-I phase present in the Li–Si/C composite

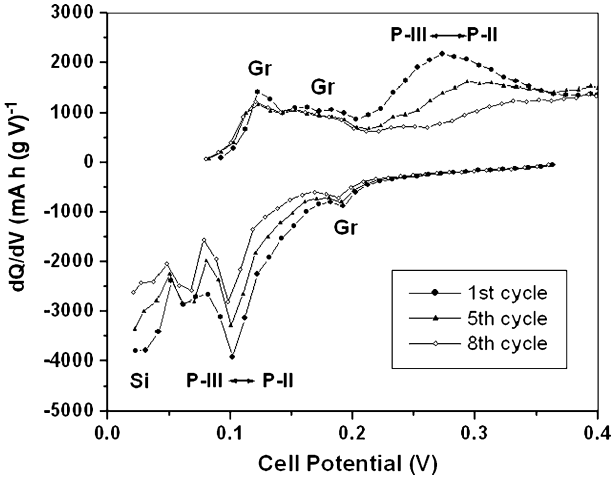

Fig. 8. Differential capacity *vs.* potential plot of Li–Si/C composite electrode, synthesized after termination the electrochemical charging reaction of Li ion with activated Si/C composite at ~0.4 V, after the 1st, 5th and 8th cycle cycled at ~160 mA g^{-1} within the potential window of 0.02–0.4 V.

synthesized at ~0.4 V to form P-II phase during lithiation, which is in good agreement with the expected phase/es at ~0.4 V (P-II) according to the metastable Li–Si phase diagram shown in Fig. 5 indicating the formation of only the P-II phase at ~0.4 V. The differential capacity plot of Li–Si/C composite generated at ~0.4 V shows that the peak intensity corresponding to the alloying and dealloying processes of P-II ↔ P-III, associated with peak potential ~0.1 V during discharge and ~0.27 V during charge, decreases in subsequent cycles. This therefore suggests that the driving force in the potential window (~0.02–0.4 V) is not strong enough to activate the alloying and dealloying reaction between the P-II (Li–30 at.% Si; Li_7Si_3) and P-III (Li–24 at.% Si; $Li_{3.16}Si$) phases at the current rate of ~160 mA g^{-1} employed for cycling, and as a result there is also a significant fade in capacity which occurs during the alloying and dealloying processes between P-II and P-III. It must be noted that the P-III phase composition is very close to the eutectic composition represented in the equilibrium Li–Si phase diagram while the P-II phase represents a congruently melting intermetallic whose phase fields are in close proximity representing only a 6 at.% difference in the Si content. The phase stability and ensuing kinetics represented by the electrochemical reactions occurring at the current rate of 160 mA g^{-1} might also preclude the reversible transformations between these two phases in the voltage range of 0.4–0.02 V. A more rigorous analysis of the phase transitions occurring in this voltage range will be needed to identify the reduced driving force for the phase transitions in this reduced voltage window range.

The present results nevertheless, clearly show that the electrochemically *in situ* generated Li–Si/C composites comprised of the alloyed Li–Si phase/es existing as a dispersoid in the C matrix, improve the stability of the electrode cycled in their stable potential window in comparison to the unalloyed and non-lithiated pure Si/C composite cycled in the potential window of 0.02–1.2 V. The long term stability and the reversible specific capacity of the Li–Si/C composites, however, can be better understood by considering the volume expansion/contraction during alloying/dealloying processes of Li–Si/C composite which depends mainly on the composition of the specific Li–Si–C alloy as well as the nature of the phase/phases present in the Li–Si/C composite. The favorable Li–Si alloy compositions, identified in this current study which exhibits a high specific capacity combined with excellent cyclability must be above 30 at.% Si (generated at ~0.4 V). The metastable electrochemical phase diagram, shown in Fig. 5, shows the formation of pure P-I and P-II phase at ~0.6 and ~0.4 V, respectively, of composition close to Li–50 at.% Si (LiSi) and Li–30 at.% Si (Li_7Si_3), respectively. On the other hand, a two phase mixture of P-I and P-II phase is expected to be formed in the potential range of 0.4–0.6 V as shown in Fig. 5. Hence, in the composition range of 30 at.% Si–50 at.% Si, the Li–Si alloy, formed by solid state electrochemical diffusion reaction of *a*-Si with Li ion at room temperature, is mainly comprised of an intimate phase mixture of P-I phase of composition Li–50 at.% Si and P-II phase of composition Li–30 at.% Si as shown in the metastable Li–Si binary alloy phase diagram at the bottom of Fig. 9 at room temperature. In the present study, the crystal structure and molar volume of P-I, P-II and P-III phase of composition Li–50 at.% Si, Li–30 at.% Si and Li–24 at.% Si, respectively, is assumed to be very similar corresponding to the intermetallic phases, LiSi, Li_7Si_3 and $Li_{13}Si_4$ indicated in the phase diagram corresponding to compositions close to P-I, P-II and P-III, respectively. Based on the reported crystal structure and molar volume of the equi-atomic composition, LiSi [39], the calculated volume expansion per mole of Si during alloying of Li with LiSi to form $Li_{13}Si_4$ along with the associated theoretical specific capacity is shown in Table 2. Hence, the reversible alloying and dealloying of Li ion with P-I or P-II phase to form P-III phase is expected to undergo a volume expansion of ~114% and ~31% with a theoretical specific capacity ~2154 and ~877 mA h g^{-1}, respectively (Table 2 and Fig. 9). We can also further assume that the specific capacity

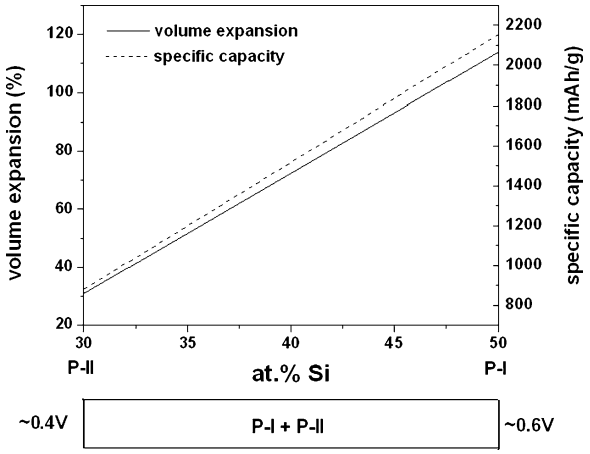

Fig. 9. Li–Si metastable phase diagram expected to be obtained by the solid state diffusion reaction of *a*-Si with Li in the composition range of 30–50 at.% Si, and the associated theoretical specific capacity and volume expansion per mole of Si to form P-III phase of composition Li–24 at.% Si by solid state electrochemical diffusion reaction of Li ion with P-I and P-II of composition Li–50 at.% Si and Li–30 at.% Si, respectively.

and the volume expansion of the phase mixture (P-I and P-II) would likely follow a simple rule of mixtures, i.e., $X = V_I X_I + V_{II} X_{II}$, where X and V denote the specific property such as specific capacity or volume expansion, and volume fraction of the respective components, respectively. Hence, the specific capacity and volume expansion can be expected to increase with increase in the volume fraction of P-I and decrease in the volume fraction of the P-II as shown in Fig. 9. In other words, with increase the atomic percent of Si in the Li–Si alloy, the specific capacity of Li–Si/C composite is expected to increase whereas the stability of the composite is expected to decrease, which is in good agreement with the present investigation and reports in the literature.

On the other hand, it should be noted that the charge potential of the Li–Si/C anode synthesized electrochemically *in situ*, comprised of the alloys in the Li–Si system as a dispersoid, will be reduced by decreasing the atomic percent of Si in the Li–Si alloy (Fig. 9) in the composition range of ~30–50 at.% Si. A reduction in the charge potential of the anode comprised of Li–Si/C composite will, however, result in a higher discharge potential in the case of the system when used in a full cell configuration utilizing a suitable lithium transition metal oxide or lithium iron phosphate cathode (cell potential = cathode potential – anode potential). The specific capacity and the energy density of a full cell, comprised of the Li–Si/C composite synthesized electrochemically *in situ* as an anode of different Li–Si alloy compositions with their stable charge potential, and M_xO_y as a cathode of average discharge potential ~4.2 V and specific capacity ~140 mA h g^{-1}, is shown in Table 3. The specific capacity of the full cell has been calculated in terms of the corresponding anode and cathode capacity as follows, $C_T = C_A C_C/(C_A + C_C)$, where C_A and C_C are the anode and cathode capacities, respectively [1,19]. Table 3 shows that the Li–Si/C composite of composition 64 at.% C–21.6 at.% Li–14.4 at.% Si, generated electrochemically at ~0.5 V, comprised of Li–Si alloy as a dispersoid of composition in the vicinity of ~Li–40 at.% Si, existing as a mixture of P-I and P-II phases, in the C matrix is the best suitable material to obtain a high energy density in the full cell configuration with excellent stability (~0.13%) despite the specific capacity of the anode being reduced by 31% (~700 mA h g^{-1}) with respect to pure Si/C composite (~1019 mA h g^{-1}). Therefore, a higher discharge potential of the full cell, comprised of the alloyed Li–Si/C based composite anode with a suitable cathode, is expected to enhance the deliverable energy density of the full cell in spite of the lower specific capacity of the Li–Si/C composite with respect

Table 3
The theoretical specific capacity and the energy density of a full cell comprised with Li–Si/C composite as an anode of different Li–Si alloy compositions and M_xO_y as a cathode of average discharge potential ~4.2 V with a specific capacity ~140 mA h g^{-1}.

Alloys	Composition	Composition of Li–Si alloy	Phase/phases	Anode specific capacity (mA h g^{-1})	Capacity loss per cycle (%)	Charge potential (V) of anode	Discharge potential (V) of full cell	Specific capacity of full cell (mA h g^{-1})	Theoretical energy density (W h kg^{-1})
Si/C	82.6 at.% C–18.4 at.% Si	–	Si + C	~1000	0.34	1.2 V	3 V	~123	~369
Li–Si/C (~0.6 V)	69 at.% C–15.5 at.% Li–15.5 at.% Si	Li–50 at.% Si	P-I (LiSi) + C	~800	0.21	0.6 V	3.6	~119	~429
Li–Si/C (~0.5 V)	64 at.% C–21.6 at.% Li–14.4 at.% Si	Li–40 at.% Si	P-I (LiSi) + P-II (Li_7Si_3) + C	~700	0.13	0.5 V	3.7	~117	~432
Li–Si/C (~0.4 V)	57.1 at.% C–30 at.% Li–12.9 at.% Si	Li–30 at.% Si	P-II (Li_7Si_3) + C	~440	3.6	0.4 V	3.8	~106	~403
C	–	–	C	~320	~0%	1.2	3	~98	~292
Si	–	–	Si	~4000	–	1.2	3	~135	~406

to the pure unalloyed Si/C composite. It must also be mentioned here however, that the electrochemical results of the Li–Si/C composite, synthesized by controlled electrochemical reaction of Li ion with Si/C composite generated by HEMM, presented in this article is essential in demonstrating the feasibility of the Li–Si/C composite as a potential anode material for lithium ion batteries. Furthermore, to realize the true potential of these systems demonstrated herein for practical application of Li–Si/C composite as an anode, it will be necessary to synthesize Li–Si alloys of preferable compositions with desirable phase/phases by non-equilibrium solid state diffusion reaction techniques, such as mechanically or chemically driven solid state processing techniques [25,40], other than *in situ* electrochemical reaction methods. There will also be a need to disperse the prepared Li–Si alloy homogeneously within the C matrix in order to obtain the desired electrochemical properties. Identification of an economically feasible synthesis technique for generating these alloyed Li–Si/C composites will therefore be a key factor in demonstrating the true potential of these systems as anodes for next generation lithium ion systems. Identification of a suitable method to generate composites of Si and C containing lithium will therefore be necessary to exploit the true potential of these systems obtained by charging the composite electrode to a reduced charge potential thus resulting in a reduced potential cycling window for the anode which in effect results in higher energy density due to the larger full cell operating voltage as explained above and shown in Table 3. This remains a challenge for the solid state chemists and the materials scientists which hopefully will be met in the near future with rapid advances being made in the science and engineering of materials synthesis and processing technologies.

4. Conclusion

Composites based on Li–Si alloy, graphite and PAN derived amorphous carbon, generated electrochemically *in situ* denoted as Li–Si/C, have been studied as a suitable anode material for lithium ion batteries. The *in situ* electrochemically synthesized Li–Si/C composites of different compositions has been synthesized by terminating the electrochemical charging reaction of Li ion following electrochemical activation of the Si/C composites generated by high energy mechanical milling (HEMM) at different potentials (~0.6, ~0.5 and ~0.4 V). The Si/C composite has been synthesized by high energy mechanical milling of graphite and silicon particles in the presence of the polyacrylonitrile (PAN) followed by thermal treatment of mechanically milled powder at 1073 K for 6 h. The Li–Si/C composite generated electrochemically *in situ* at ~0.6, ~0.5 and ~0.4 V is comprised of Li–Si alloy dispersed in graphite matrix. The overall composition of Li–Si/C composite generated at ~0.6, ~0.5 and ~0.4 V, is estimated to be close to 69 at.% C–15.5 at.% Li–15.5 at.% Si, 64 at.% C–21.6 at.% Li–14.4 at.% Si and 57.1 at.% C–30 at.% Li–12.9 at.% Si, respectively, with Li–Si alloy composition Li–50 at.% Si, Li–40 at.% Si and Li–30 at.% Si, respectively. The electrochemical studies of the electrochemically synthesized Li–Si/C composite and pure Si/C reveal that the Li–Si/C composite synthesized at ~0.6 and ~0.5 V, cycled within their stable potential window, exhibit better cyclability in comparison to pure Si/C composite cycled in the potential window of 0.02–1.2 V. On the other hand, the specific capacity of the Li–Si/C composite synthesized at ~0.6 and ~0.5 V is ~19% (819 mA h g^{-1}) and ~31% (~700 mA h g^{-1}) lower, respectively, than pure Si/C composite (~1019 mA h g^{-1}). However, it is expected that the energy density of a full cell configuration, comprised of the *in situ* synthesized Li–Si/C composite coupled with a suitable cathode, is higher than the Si/C composite coupled with the same cathode due to the expected improvements in the energy density due to a higher discharge potential for the full cell. It has been identified that the Li–Si/C composite of composition 64 at.% C–21.6 at.% Li–14.4 at.% Si, generated at ~0.5 V, comprised of Li–Si alloy as a dispersoid of composition in the vicinity of ~Li–40 at.% Si, is the best suitable material for anode to obtain a high energy density in the full cell configuration with excellent stability (~0.13%) despite the specific capacity of the anode (~700 mA h g^{-1}) being reduced by 31% with respect to the pure Si/C composite (~1019 mA h g^{-1}). This study therefore demonstrates a new concept on the use of Li–Si alloys, dispersed homogeneously in a carbon matrix, as new potential anodes that can be explored in a reduced voltage window exhibiting excellent capacity retention without compromising on the overall energy density.

Acknowledgements

The authors gratefully acknowledge the financial support of the DOE-BATT program and partial support of the Ford Foundation. The authors also acknowledge the Edward R. Weidlein Chair Professorship funds for partial support of this research.

References

[1] U. Kasavajjula, C. Wang, A.J. Appleby, J. Power Sources 163 (2007) 1003.
[2] C.K. Chan, H. Peng, G. Liu, K. Mcilwrath, X.F. Zhang, R.A. Huggins, Y. Cui, Nat. Nanotechnol. 3 (2008) 31.
[3] J.L. Tirado, Mater. Sci. Eng. R 40 (2003) 103.
[4] Annual Progress Report for Energy Storage and Development, U. S. Department of Energy, Vehicle Technologies Program, 2007, Washington, D.C.
[5] L.Y. Beaulieu, K.W. Eberman, R.L. Turner, L.J. Krause, J.R. Dahn, Electrochem. Solid State Lett. 4 (2001) A137.
[6] J.H. Ryu, J.W. Kim, Y.E. Sung, S.M. Oh, Electrochem, Solid State Lett. 7 (2004) A306.
[7] J.P. Maranchi, A.F. Hepp, A.G. Evans, N.T. Nuhfer, P.N. Kumta, J. Electrochem. Soc. 153 (2006) A1246.
[8] O. Mao, R.L. Turner, I.A. Courtney, B.D. Fredericksen, M.I. Buckett, L.J. Krause, J.R. Dahn, Electrochem, Solid State Lett. 2 (1999) 3.
[9] I.-S. Kim, G.E. Blomgren, P.N. Kumta, J. Power Sources 130 (2004) 275.
[10] I.-S. Kim, P.N. Kumta, G.E. Blomgren, Electrochem. Solid State Lett. 3 (2000) 493.
[11] X.N. Zhang, G.L. Pan, G.R. Li, J.Q. Qu, X.P. Gao, Solid State Ionics 178 (2007) 1107.
[12] M.K. Datta, P.N. Kumta, J. Power Sources 158 (2006) 557.
[13] H. Uono, B.C. Kim, T. Fuse, M. Ue, J. Yamaki, J. Electrochem. Soc. 153 (2006) A1708.
[14] W. Wang, M.K. Datta, P.N. Kumta, J. Mater. Chem. 17 (2007) 3229.
[15] M.K. Datta, P.N. Kumta, J. Power Sources 165 (2007) 368.
[16] A. Timmons, A.D.W. Todd, S.D. Mead, G.H. Carey, R.J. Sanderson, R.E. Mar, J.R. Dahn, J. Electrochem. Soc. 154 (2007) A865.
[17] W. Wang, P.N. Kumta, J. Power Sources 172 (2007) 650.
[18] J. Saint, M. Morcrette, D. Larcher, L. Laffont, S. Beattie, J.P. Peres, D. Talaga, M. Couzi, J.M. Tarascon, Adv. Funct. Mater. 17 (2007) 1765.
[19] M. Yoshio, T. Tsumura, N. Dimov, J. Power Sources 146 (2005) 10.
[20] P. Guo, G. Yin, Y. Ma, Electrochim. Acta 52 (2007) 4878.
[21] H. Okamoto, in: T.B. Massalski (Ed.), Binary Alloy Phase Diagram, vol. 1, ASM International, Materials Park, OH, 1990.
[22] B.A. Boukamp, G.C. Lesh, R.A. Huggins, J. Electrochem. Soc. 128 (1981) 725.
[23] C.J. Wen, R.A. Huggins, J. Solid State Chem. 37 (1981) 271.
[24] W.J. Weydanz, M.W. Mehrens, R.A. Huggins, J. Power Sources 81/82 (1999) 237.
[25] M. K. Datta, Ph.D. Thesis, Indian Institute of Technology, Kharagpur, India, 2001.
[26] http://www.originlab.com/
[27] J. Li, J.R. Dahn, J. Electrochem. Soc. 154 (2007) A156.
[28] P. Limthongkul, Y. Jang, N.J. Dudney, Y.M. Chiang, Acta Mater. 51 (2003) 1103.
[29] M.N. Obrovac, L. Christensen, Electrochem, Solid State Lett. 7 (2004) A93.
[30] Y.M. Kang, S.M. Lee, S.J. Kim, G.J. Jeong, M.S. Sung, W.U. Choi, S.S. Kim, Electrochem. Commun. 9 (2007) 959.
[31] T.D. Hatchard, J.R. Dahn, J. Electrochem. Soc. 151 (2004) A838.
[32] H. Li, X. Huang, L. Chen, G. Zhou, Z. Zhang, D. Yu, Y.J. Mo, N. Pei, Solid State Ionics 135 (2000) 181.
[33] J. Nanda, M.K. Datta, J.T. Remillard, A. O'Neill, P.N. Kumta, Electrochem. Commun. 11 (2009) 235.
[34] B.S. Murty, M.K. Datta, S.K. Pabi, Sadhana 28 (2003) 23.
[35] Z. Ogumi, M. Inaba, in: W.A. Schalkwijk, B. Scrosati (Eds.), "Carbon Anodes" in Advances in Lithium ion Batteries, Kluwer Academic, New York, 2002, pp. 79–101.
[36] J. Maranchi, O.I. Velikokhatnyi, M.K. Datta, I.S. Kim, P.N. Kumta, in: B. Lee, S. Komarneni (Eds.), Ceramic Materials for Lithium-ion Battery Application" in Chemical Processing of Ceramics, 2nd ed., CRC Press, Taylor and Francis, 2005, p. 667.
[37] J.P. Maranchi, A.F. Hepp, P.N. Kumta, Electrochem, Solid State Lett. 6 (2003) A198.
[38] J.B. Kim, B.S. Jun, S.M. Lee, Electrochem. Acta 50 (2005) 3390.
[39] Y. Kubota, M.C.S. Escano, H. Nakanishi, H. Kasai, J. Alloys Compd. 458 (2008) 151.
[40] G. Martin, P. Bellon, Solid State Phys. 50 (1997) 189.